

Pease cite as “Kondou, C., Hrnjak, P.S., “Heat Rejection in Condensers Close to Critical Point - Desuperheating, Condensation Superheated Region and Condensation of Two Phase Fluid-”, Heat Transfer. Eng., vol. 34, no. 14, 1180-1190, (2013)”

Heat Rejection in Condensers Close to Critical Point

- De-Superheating, Condensation in Superheated Region and Condensation of Two-Phase Fluid -

CHIEKO KONDOU

Department of Mechanical Science and Engineering, University of Illinois at Urbana-Champaign, Urbana, IL 61801, USA

PEGA HRNJAK

Department of Mechanical Science and Engineering, University of Illinois at Urbana-Champaign, Urbana, IL 61801, USA

Address correspondence to Professor Pega Hrnjak, Department of Mechanical Science and Engineering, University of Illinois at Urbana-Champaign, 1206 W. Green St. 156 MechSE Bldg., Urbana, IL 61801, USA. E-mail: pega@illinois.edu

Tel.: +1 217 333 8110

Fax: +1 217 333 1942

Conventional modeling of condensers typically assumes three zones: de-superheating, condensation, and subcooling zone, even it is clear that condensation occurs in de-superheating zone at some conditions and subcooling occurs during condensation. This paper discusses the actual situation and provides experimental validation of the hypothesis. The experimental results show heat transfer coefficients (HTC) of CO₂ and R410A at mass fluxes from 100 to 240 kg m⁻²s⁻¹

¹, heat fluxes from 3 to 25 kW m⁻², and reduced pressures from 0.68 to 1.00 in a horizontal smooth tube of 6.1 mm inner diameter. Data are compared to correlations proposed for other working fluids or other conditions. Results show much higher values of HTC than correlation proposed for single-phase turbulent flow in superheat zone. The occurrence of condensation in superheat zone is evident when tube wall temperature is below saturation temperature. The results suggest that simplified calculations of heat rejection in superheated zone could oversize condensers. The semi-empirical correlation, which is here proposed as the combination of existing correlations for single-phase turbulent and saturated condensation, satisfactorily predicts HTC of the superheat zone condensation.

INTRODUCTION

Balekjian and Katz [1] experimentally investigated condensation from superheated vapors of R114 and steam on an outer surface of a horizontal tube. Their experimental HTC suggested that the lowering cooling surface temperature, below saturation point, generates condensate from superheated vapor. Altman et al. [2] provided six points of experimentally determined HTC, which are averaged from superheated inlet to saturated outlet in a test section of 1.22 m length 8.71 mm ID. With those six data having various superheat degree at test section inlet, approximately 30 to 70 % decrease in HTC from a correlation valid for two-phase zone condensation was confirmed. Bell [3] accepted that the criterion of condensation occurrence in de-superheating zone is the tube wall temperature below saturation point, and then cautioned that the simple use of LMTD

(logarithmic mean temperature difference) method to calculate the overall coefficient of condensers could be invalid. Miropolskiy et al. [4] provided experimental data for the quasi-local HTC of superheated steam vapor flowing downward in a cooled vertical smooth tube. The results experimentally presented the criterion of condensation occurrence is when the tube wall temperature is below saturation point. Further, their data showed the behavior of superheat zone condensation for various reduced pressure up to 0.82. Fujii et al. [5] experimentally investigated condensation of R11 and R113 flow in horizontal smooth tubes. From the temperature distribution in the radial direction of the horizontal middle plane of the tube, they proved coexistence of superheated vapor and subcooled liquid in condensation flow. They varied the vapor mass quality, which indicates actual vapor and liquid mass flow rate in non-equilibrium state, to analyze the mass transport process. Lee et al. [6] experimentally investigated condensation in superheated R22 vapor and proposed a physical model accounting the sensible heat on the condensation heat transfer. Their model defines HTC bulk temperature as the reference temperature. In response, Webb [7] reported that sensible heat is negligible and simplified model defines HTC with saturation temperature gives same results to Lee's model [6].

Various new types of systems and applications drive operating conditions closer to the critical point making heat rejected in superheat zone greater than in two-phase zone. Conditions just below the critical point are thus increasingly common. For instance, the most operating hours CO₂ commercial refrigeration systems accumulate from autumn to spring in subcritical conditions. That is common even in night time of summer seasons in northern climate regions. R410A water heaters or clothes dryers are becoming popular and along with few other applications operate just below

the critical point. To increase efficient operation, it is crucial to improve understanding heat transfer in condenser. Heat rejection in the condenser is typically simplistically divided in three zones: de-superheating, two-phase condensation, and single-phase subcooling. De-superheating is assumed to be heat transfer from superheated vapor in mostly turbulent single-phase conditions, where heat transfer is significantly lower than when condensation starts. The conservative estimation that ignores condensation in superheated region is not significant when heat transferred is small, as in most of the situations. However, in the conditions of interest to this paper, just below critical point as described above the size of the heat exchanger could be significantly affected by this simplification because heat rejected in de-superheating can be several times greater than in two phase condensation. That is the practical significance of this work. The authors [8] presented experimental results for only CO₂ heat rejection (cooling/condensation) flow in 6.1 mm ID smooth tube at the pressure from 5.0 to 7.5MPa. The experimental results identified the condensation in superheated vapor. In order to strengthen experimental verification, one additional refrigerant R410A was explored. It was chosen because of its importance in applications and the effect of the refrigerant properties on condensation heat transfer.

CONDENSING SUPERHEAT ZONE

Figure 1 illustrates the heat flow and the temperature profile in condensing superheat zone, where bulk mean refrigerant temperature is above saturation point. According to Soliman's flow regime [9], condensation begins as mist flow and then changes into annular flow. According to Altman et al. [2], thin ridges or droplets flow on the interior tube surface. Figure 1 explains the

heat exchange with annular flow model for simplification.

From continuity, the total mass flow rate \dot{m}_{total} of vapor and liquid refrigerant is,

$$\dot{m}_{\text{total}} = \dot{m}_{V,i} + \dot{m}_{L,i} = \dot{m}_{V,o} + \dot{m}_{L,o} \quad (1)$$

The amount of condensate generated through a segment $\Delta\dot{m}_L$ is expressed from the continuity as,

$$\Delta\dot{m}_L = \dot{m}_{L,o} - \dot{m}_{L,i} = \dot{m}_{V,i} - \dot{m}_{V,o} = \Delta\dot{m}_V \quad (2)$$

The average enthalpies in superheated vapor and subcooled liquid are represented with heat capacities Cp_V Cp_L , and degree of superheat and subcool ΔT_{SH} ΔT_{SC} .

$$\left. \begin{aligned} \bar{h}_V &= h_{V,\text{sat}} + \overline{Cp_V \Delta T_{SH}} = h_{V,\text{sat}} + \overline{\Delta h_{SH}} \\ \bar{h}_L &= h_{L,\text{sat}} - \overline{Cp_L \Delta T_{SC}} = h_{V,\text{sat}} - \Delta h_{LV} - \overline{\Delta h_{SC}} \end{aligned} \right\} \quad (3)$$

Total inlet heat at the entrance of a segment is,

$$\begin{aligned} h_{b,i} \dot{m}_{\text{total}} &= \bar{h}_{V,i} \dot{m}_{V,i} + \bar{h}_{L,i} \dot{m}_{L,i} \\ &= \left(h_{V,\text{sat}} + \overline{\Delta h_{SH,i}} \right) \dot{m}_{V,i} + \left(h_{V,\text{sat}} - \Delta h_{LV} - \overline{\Delta h_{SC,i}} \right) \dot{m}_{L,i} \end{aligned} \quad (4)$$

Similarly, the total outlet heat at the exit of a segment is,

$$\begin{aligned} h_{b,o} \dot{m}_{\text{total}} &= \bar{h}_{V,o} \dot{m}_{V,o} + \bar{h}_{L,o} \dot{m}_{L,o} \\ &= \left(h_{V,\text{sat}} + \overline{\Delta h_{SH,o}} \right) (\dot{m}_{V,i} - \Delta\dot{m}_L) \\ &\quad + \left(h_{V,\text{sat}} - \Delta h_{LV} - \overline{\Delta h_{SC,o}} \right) (\dot{m}_{L,i} + \Delta\dot{m}_L) \end{aligned} \quad (5)$$

The subtraction from Eq. (5) to Eq. (4) gives the total heat exchange through a segment.

$$\begin{aligned} & (h_{b,i} - h_{b,o}) \dot{m}_{\text{total}} \\ &= \underbrace{\left(\overline{\Delta h_{SH,i}} - \overline{\Delta h_{SH,o}} \right) \dot{m}_{V,i} + \overline{\Delta h_{SH,o}} \Delta\dot{m}_L}_{SH} \\ &\quad + \underbrace{\Delta h_{LV} \Delta\dot{m}}_{latent} + \underbrace{\left(\overline{\Delta h_{SC,o}} - \overline{\Delta h_{SC,i}} \right) \dot{m}_{L,i} + \Delta h_{SC,o} \Delta\dot{m}_L}_{SC} \end{aligned} \quad (6)$$

In the right of Eq. (6), the first, second, and third terms shows heat transfer rate caused by de-superheating of vapor flow, latent heat rejection to generate condensate, and subcooling of

condensate.

$$\dot{Q}_{\text{total}} = \dot{Q}_{\text{SH}} + \dot{Q}_{\text{latent}} + \dot{Q}_{\text{SC}} \quad (7)$$

$$q_{\text{total}} = q_{\text{SH}} + (q_{\text{latent}} + q_{\text{SC}}) \quad (8)$$

The driving temperature difference for the heat flux caused by de-superheating q_{SH} is probably the difference from bulk temperature to saturation temperature on the liquid film surface ($T_{\text{rb}} - T_{\text{sat}}$). The remaining summation of heat fluxes ($q_{\text{latent}} + q_{\text{SC}}$) is manipulated as a heat flux by saturated condensation. Because condensation requires degree of subcool of cooling surface, the HTC of saturated condensation α_{TP} always includes both heat fluxes. That driving temperature difference is normally taken as a difference from saturation temperature to wall temperature ($T_{\text{sat}} - T_{\text{wi}}$). Under the assumption of same heat transfer area for de-superheating and saturated condensation (that means thin liquid film), Eq. (8) could be converted with those HTCs driving temperature differences to,

$$\alpha (T_{\text{rb}} - T_{\text{wi}}) \approx \alpha_{\text{SH}} (T_{\text{rb}} - T_{\text{sat}}) + \alpha_{\text{TP}} (T_{\text{sat}} - T_{\text{wi}}) \quad (9)$$

EXPERIMENTAL SETUP AND METHOD

Figure 2 shows the schematic diagram of experimental apparatus. The refrigerant loop mainly consists of a variable speed gear pump, a coriolis-type mass flow meter, an electric pre-heater, a mixer, a pre-cooler, a test section, two after-coolers, and receiver tank. In a mixer placed at entrance of the pre-heater, pressure and bulk-mean temperature of superheated vapor are measured. System pressure is adjusted roughly by refrigerant charge amount and precisely by inlet temperature and flow rate of cooling water flow through the after-coolers.

Test Section and Test Tube

Figure 3 (a) and (b) show a structure of the test section and dimensions of the test tube. The test tube, which is a smooth copper tube of 6.1 mm ID and 9.53 mm OD, is placed horizontally and covered with a thick brass jacket. The halved brass jacket is pressed over the test tube and the small gap between them is filled with a thermal paste. On the outside of the brass jacket, copper tubes are attached with solder allowing cooling water to flow through. This structure yields cooling conditions with an almost uniform temperature. Twelve thermocouples are embedded into the top, bottom, right, and left of the test tube wall at three positions in an axial direction. The active cooling length by the brass jacket is 150 mm, which is relatively short for measuring quasi-local HTC in axial direction.

Experimental Procedure

When measuring heat transfer in superheat zone refrigerant superheat at the test section inlet is controlled from 5 to 40 K by pre-heater; meanwhile, water flow of pre-cooler is shut. During measurements in two-phase zone and superheat zone below 5 K of superheat, superheated fluid flow through the mixer is kept approximately 5 K for finding bulk enthalpy; meanwhile, inlet condition of the test section is controlled by flow rate and inlet temperature of cooling water flow through the pre-cooler.

Data Reduction Procedure

Figure 3 (c) explains the data reduction method. The main measured values are the refrigerant mass flow rate \dot{m}_r , bulk-mean temperature $T_{rb,MC}$, and absolute pressure P_{MC} in the mixer, the bulk water temperature of pre-cooler inlet $T_{H_2O,PCi}$ and outlet $T_{H_2O,PCo}$, test section inlet $T_{H_2O,TSi}$ and outlet $T_{H_2O,TSo}$, and the water mass flow rate of pre-cooler $\dot{m}_{H_2O,PC}$ and test section $\dot{m}_{H_2O,TS}$. The bulk-mean enthalpy in the mixer $h_{rb,MC}$ is determined from $T_{rb,MC}$ and P_{MC} using the function of equilibrium state provided by RefpropVer.8.0 [10]. The enthalpy changes through the pre-cooler Δh_{PC} and the test section Δh_{TS} are obtained by water side heat balances as below.

$$\Delta h_{PC} = \left[(T_{H_2O,PCo} - T_{H_2O,PCi}) \dot{m}_{H_2O,PC} C_{p,H_2O} - \dot{Q}_{gain,PC} \right] / \dot{m}_r \quad (10)$$

$$\Delta h_{TS} = \left[(T_{H_2O,TSo} - T_{H_2O,TSi}) \dot{m}_{H_2O,TS} C_{p,H_2O} - \dot{Q}_{gain,TS} \right] / \dot{m}_r \quad (11)$$

where $\dot{Q}_{gain,PC}$ and $\dot{Q}_{gain,TS}$ are preliminarily measured heat leak from ambient air through the insulators. The bulk mean temperature at the test section T_{rb} is obtained from bulk enthalpy and pressure with the equilibrium state function of RefpropVer.8.0 [10].

$$\left. \begin{aligned} T_{rb} &= (T_{rb,i} + T_{rb,o}) / 2 \\ T_{rb,i} &= f_{equilibrium} (h_{b,MC} - \Delta h_{PC}, P_{MC} - \Delta P_{PC}) \\ T_{rb,o} &= f_{equilibrium} (h_{b,MC} - \Delta h_{PC} - \Delta h_{TS}, P_{MC} - \Delta P_{PC} - \Delta P_{TS}) \end{aligned} \right\} \quad (12)$$

The average heat flux of the test section on the interior tube wall q_{wi} is,

$$q_{wi} = \frac{(T_{H_2O,TSo} - T_{H_2O,TSi}) \dot{m}_{H_2O,TS} C_{p,H_2O} - \dot{Q}_{gain,TS} - \dot{Q}_{cond}}{(d_i \cdot \pi \cdot \Delta Z_\alpha)} \quad (13)$$

where \dot{Q}_{cond} is the conduction heat from outside the cooling brass jacket estimated numerically for each condition. Procedure of numerical analysis and typical results on \dot{Q}_{cond} are specified in Reference [8]. The definition of average heat transfer coefficient α is,

$$\alpha = \frac{q_{wi}}{\Delta T}, \quad \Delta T = T_{rb} - T_{wi} \quad (14)$$

where T_{wi} is the average temperature of the 12 points in the tube wall. The reference refrigerant temperature is defined as an arithmetic mean of inlet and outlet bulk temperatures $T_{rb,i}$ $T_{rb,o}$, which are found from each pressure P_{TSi} and P_{TSo} and enthalpies $h_{b,i}$ and $h_{b,o}$. With this method, driving temperature difference ΔT in superheat zone is defined as “bulk-to-wall temperature difference” ($T_{rb} - T_{wi}$). Then this continuously changes into “saturation-to-wall temperature difference” ($T_{sat} - T_{wi}$) at the thermodynamic vapor quality 1.0 for two-phase zone.

Table 1 lists the measurement uncertainties obtained from the results of two standards deviation of calibration, resolution of data loggers and calibration tools, and the stability of excitation voltages. Combined measured uncertainties are calculated from those uncertainties in conformity of Refs. [11] and [12]

RESULTS AND DISCUSSION

Identification of Condensation from Superheated Vapor

Figure 4 shows experimental results for temperature and derived HTC compared to selected correlations. Figure 4 (a) is R410A at 2.7 MPa, $200 \text{ kg m}^{-2}\text{s}^{-1}$, and 10 kW m^{-2} , which is the typical condition for A/C condensers in summer season. Figure 4 (b) and (c) are the results of R410A and CO_2 at same reduced pressure $P/P_{crit}= 0.81$. The horizontal axes show the bulk-mean enthalpy h_b and the top axes in upper graphs show vapor quality x_b . These are obtained from bulk mean temperature of superheated vapor $T_{b,MC}$ under the assumption of equilibrium. The upper graphs show the bulk-mean refrigerant temperature of the test section inlet $T_{rb,i}$ and outlet $T_{rb,o}$, and averaged tube wall temperatures T_{wi} . The center graphs show the representative temperature

difference $(T_{rb,i} + T_{rb,o})/2 - T_{wi}$. The bottom graphs show the average HTC α of the test section and five comparative correlations. The bars show measurement uncertainties vertically and enthalpy changes through the test section horizontally.

As shown in Figure 4 (b), this study specifically categorizes the heat rejection process as superheat, two-phase, and subcool zone where the bulk-mean refrigerant temperature is superheated, saturated, and subcooled, respectively. The dashed lines in Figure 4 are selected correlations of Gnielinski [13] with Petukov's correction factor [14] for superheat zone, Cavallini et al. [15] for two-phase zone, and Gnielinski [13] with Sieder-Tate's correction factor [16] for subcool zone.

As shown in Figure 4 (a), experimental HTC starts gradually increasing from Gnielinski's correlation when the average temperature of tube wall T_{wi} reaches saturation point. This start point strongly supports the identification of condensation in presence superheated vapor. Thus, the superheat zone could be subdivided into single-phase superheat zone (I) and condensing superheat zone (II) by condensation occurrence.

Modification of the Saturated Condensation Correlation near Critical Point

Figure 5 (a) shows the change of experimental and predicted HTC of CO₂ condensation across the critical point 7.4 MPa, and 344 kJ kg⁻¹. Figure 5 (b) is HTC of R410A across the critical point 4.9 MPa, and 368 kJ kg⁻¹. As shown with dashed line and symbols, predicted HTC by Cavallini's correlation [15] shows excellent agreement with the experimental data. Nevertheless, it deviates from the experimental data at high reduced pressure P/P_{crit} from 0.82 to 1.0. This is anticipated

because the range of reduced pressure was not included in original correlation. To correct Cavallini's correlation at these high reduced pressures, following methodology is discussed. Fujii et al. [17] [18] theoretically verified extension of Nusselt's film-wise condensation theory [19] up to reduced pressure 0.995 by using liquid properties evaluated at the film temperature but not saturation temperature.

Figure 6 shows the calculation results of CO₂ specific heat from the tube wall to liquid surface at the 6, 7 and 7.36 MPa, and temperature difference 5 K. For the calculation, it is assumed that the temperature distribution in the liquid film is linear and the liquid surface is saturation condition. Near the critical pressure at 7.36 MPa, specific heat drastically increases towards the liquid surface. Similarly, thermal conductivity and Prandtl number increase while viscosity and density decrease. Therefore selection of characteristic temperature for liquid properties becomes even more important near the critical point. Following equation is here proposed modification of Cavallini's correlation with \overline{Cp}_L , as shown in Figure 6, and film temperature.

$$\begin{aligned}
J_G &= x_b G_r / \sqrt{g d_i \rho_{Vsat} (\rho_{Lsat} - \rho_{Vsat})} \\
J_G^T &= \left\{ (7.5/4.3 X_{tt}^{1.111} + 1)^{-3} + 2.6^{-3} \right\}^{-1/3} \\
X_{tt} &= \left(\frac{\mu_{Lsat}}{\mu_{Vsat}} \right)^{0.1} \left(\frac{\rho_{Vsat}}{\rho_{Lsat}} \right)^{0.5} \left(\frac{1-x_b}{x_b} \right)^{0.9} \\
\alpha_{LO_f} &= 0.023 (G_r d_i / \mu_{L_f})^{0.8} Pr_{L_f}^{0.4} (\lambda_{Lsat} / d_i) \\
Pr_{L_f} &= (\bar{Cp}_L \mu_{L_f}) / \lambda_{L_f} \\
\bar{Cp}_L &= (h_{Lsat} - h_{Lwi}) / (T_{sat} - T_{wi}) \\
\alpha_{Nusselt_f} &= 0.725 \left[\frac{\lambda_{L_f}^3 \rho_{L_f} (\rho_{L_f} - \rho_{Vsat}) g \Delta h_{LV}}{\mu_{L_f} d_i (T_{sat} - T_{wi})} \right]^{0.25} \\
\alpha_{strat} &= \alpha_{Nusselt_f} \left\{ 1 + 0.741 \left(\frac{1-x_b}{x_b} \right)^{0.3321} \right\}^{-1} + (1-x_b)^{0.087} \alpha_{LO_f} \\
\alpha_{TP} &= \begin{cases} J_G > J_G^T : \alpha_A = \alpha_{LO_f} \left[1 + 1.128 x_b^{0.8170} \left(\frac{\rho_{Lsat}}{\rho_{Vsat}} \right)^{0.3685} \right. \\ \quad \times \left. \left(\frac{\mu_{Lsat}}{\mu_{Vsat}} \right)^{0.2363} \left(1 - \frac{\mu_{Vsat}}{\mu_{Lsat}} \right)^{2.144} Pr_{L_f}^{-0.1} \right] \\ J_G \leq J_G^T : \left[\alpha_A (J_G^T / J_G)^{0.8} - \alpha_{strat} \right] (J_G / J_G^T) + \alpha_{strat} \end{cases} \quad (15)
\end{aligned}$$

where, subscript “_f” indicates the value evaluated at the film temperature which is the modified value from the original correlation. As shown with solid line in Figures 5 (a) and (b), this modified correlation satisfactorily agrees with experimental HTC at reduced pressures up to 0.975 for CO₂ and R410A both.

Proposal of a Prediction Method for Condensing SH Zone

From Eq. (10), HTC in condensing superheat zone is expressed as,

$$\alpha_{\text{total}} = [\alpha_{\text{SH}}(T_b - T_{\text{sat}}) + \alpha_{\text{TP}}(T_{\text{sat}} - T_{\text{wi}})] / (T_b - T_{\text{wi}}) \quad (16)$$

Here, α_{TP} is calculated by modified Cavallini's correlation Eq. (15). However, the assumption of same flow regime as vapor quality 1.0 is required for solving the equation. As a computational procedure, Martinelli parameter X_{tt} , dimensionless gas velocity J_G and J_G^{T} , and fully-stratified HTC α_{strat} , were calculated same as when vapor quality at 0.995. In the correct way, the correlation should be newly developed with actual vapor mass quality accounting non-equilibrium condition. However, this concept requires multiple iterations and might not be worth for the calculation for only superheat zone. In order to avoid further computational load and iteration errors, this paper recommends above supplement method with existing correlations. Next, α_{SH} is calculated by the correlation Gnielinski [13] with Petukov's correction factor F_a [14] assuming the effect of entrainment or complex interface between vapor and liquid is negligible.

$$\begin{aligned} \alpha_{\text{SH}} &= Nu_0 F_a (\lambda_b / d_i), \quad F_a = (T_{\text{wi}} / T_{\text{rb}})^{-0.36} \\ Nu_0 &= \frac{(f_b / 8)(G_r d_i / \mu_b - 1000) Pr_b}{1 + 12.7(f_b / 8)^{1/2} (Pr_b^{2/3} - 1)} \\ f_b &= [1.82 \cdot \log_{10}(G_r d_i / \mu_b) - 1.64]^{-2} \end{aligned} \quad (17)$$

where f_b is Filonenko's friction factor [20].

Calculation Procedure from Superheat Zone to Subcool Zone

Figure 7 shows the overview of calculation procedure. The start point of condensation $h_{\text{b,start}}$ was found by binary search method with the criterion $T_{\text{wi}} = T_{\text{sat}}$ and Eq. (17). At vapor quality 1.0, the tube wall temperature $T_{\text{wi,end}}$ is found by Eq. (15). The line connects two points $(h_{\text{b,start}}, T_{\text{sat}})$ and $(h_{\text{v}}, T_{\text{wi,end}})$ is obtained from first order approximation. As shown with solid lines in Figure 4,

this approximation satisfactorily agrees with experimental data and allows reducing one loop of iteration. HTC in subcool zone α_{SC} is predicted by Gnielinski [13] with Sieder and Tate's correction factor F_a [16] as below.

$$\alpha_{SC} = Nu_0 F_a (\lambda_b / d_i), \quad F_a = (\mu_b / \mu_{wi})^{0.14} \quad (18)$$

When reduced pressure P/P_{crit} is above 0.9 and refrigerant mass flux G_r is above $150 \text{ kg m}^{-2}\text{s}^{-1}$, Eq. (18) gives higher HTC than experimental HTC and Eq. (15) at vapor quality 0. The radial properties change becomes too drastic to be corrected by Sieder and Tate's factor. For better interrelating between two-phase zone and subcool zone, below correlation using Pr_{L-f} is better to applied.

$$\begin{aligned} &P/P_{crit} > 0.9 \text{ and } G_r > 150 \text{ kg m}^{-2}\text{s}^{-1}: \\ &\alpha_{SC} = Nu_f (\lambda_{L-f} / d_i) \\ &Nu_f = \frac{(f_f/8)(G_r d_i / \mu_{L-f} - 1000) Pr_{L-f}}{1 + 12.7 (f_f/8)^{1/2} (Pr_{L-f}^{2/3} - 1)} \\ &f_f = \left[1.82 \cdot \log_{10} (G_r d_i / \mu_{L-f}) - 1.64 \right]^{-2} \end{aligned} \quad (19)$$

Comparison between Calculation and Experimental Results

Predicted temperatures and HTC by the above method are shown with solid lines in Figure 4. As the comparison, above calculation results satisfactorily agree with experimental results of R410A and CO₂ both despite of the audacious simplifications on α_{SH} and α_{TP} in the zone, where condensation occurs in superheated vapor. The remarkable improvement is the tube wall temperature of the condensing superheat zone. The existing prediction, which does not account condensation, gives over 10 K lower tube wall temperature near vapor quality 1.0 and it is not

negligible deviation for circuit design of condensers. Compared with this, the newly proposed method predicts the temperature with accuracy within 2 K approximately.

Figure 8 compares the experimental HTC of various heat fluxes to the correlations Eqs. (15) to (19) and shows the effect of heat flux on the start point of condensation. Since tube wall temperature tends to be lower at higher heat flux, the temperature reaches saturation point earlier and condensation starts earlier with increasing heat flux. This tendency is predicted by the proposed correlations and the curve of calculation results overlaps experimental data point satisfactorily in the zone of condensing superheat.

Comparison of HTC between CO₂ and R410A at the Same Reduced Pressure

Figure 9 shows HTC of CO₂ in the three left graphs and R410A in the right graphs at 100 kg m⁻²s⁻¹, 10 kW m⁻², and reduced pressures P / P_{crit} 0.68, 0.81 and 0.95. Each saturation temperature T_{sat} and latent heat Δh_{LV} is shown with the conditions in those graphs. Vertical dashed line divides zones into single-phase superheat, condensing superheat, two-phase, and subcool from right to left. Symbols show experimental HTC, and thick solid lines are calculated HTC by Eqs. (15) to (19).

In single-phase superheat zone, HTC of CO₂ is barely higher than R410A at the same reduced pressure. In two-phase zone, HTC of CO₂ exceeds R410A. HTC almost always has maximum at the border between two-phase and superheat zone ($x_b = 1$). The maximum HTC of CO₂ is roughly 120 to 170 % of R410A at the reduced pressure from 0.68 to 0.95. As Nusselt's film wise condensation theory describes, latent heat Δh_{LV} is one of important factor on condensation HTC. Larger latent heat means that released heat from a mass of vapor is larger at the moment of phase

change and increases condensation HTC. As noted in the graphs, the latent heat of CO₂ is roughly 140% of R410A and this increases HTC in two-phase zone. Although experimental HTC and calculated HTC satisfactorily agree in general, experimental HTC of R410A slightly deviates when approaching critical point and is approximately 25% below from correlation at reduced pressure 0.95.

Summary of Experimental Results and Correlations through the Superheat, Two-Phase, and Subcool Zone

Figure 10 shows experimental and predicted HTC of various pressures of CO₂ and R410A. In four graphs of Figures 10 (a) and (b), symbols show experimental HTC and solid lines show the newly proposed correlation Eqs. (15) to (19) at the constant pressures. The predicted HTC by newly proposed correlation agrees with experimental HTC for both refrigerant and condition. Figure 10 plots HTC data on the P - h diagram for the purpose of exhibiting the portion of condensing superheat zone in entire enthalpy change through a condenser inlet to outlet. For instance, when a condenser inlet to outlet temperature of R410A system is 90 °C to 45 °C at 2.7 MPa, the enthalpy change in condensing superheat zone is approximately 14%. At 4.6 MPa, the enthalpy change is approximately 21%. Likewise, the enthalpy change ratio of condensing superheat zone to the entire heat rejection becomes larger and important for condenser design.

Similarity between Supercritical and Subcritical Heat Rejection Process

Figure 10 (a) includes some HTC data of CO₂ at 7.5 MPa, just above the critical pressure. In

the graph of CO₂ at 7.5 MPa, solid lines show correlations by Gnielinski [13], Petrov and Popov [21]. Gnielinski correlation, which is valid at subcritical pressure, shows higher HTC than experimental data especially around the pseudo-critical point 350 kJ kg⁻¹. This is due to the drastic property change in radial direction. The other correlation by Petrov and Popov [21] takes account into consideration the strong radial property change. Hence the maximum HTC of Petrov and Popov's correlations are much closer to the experimental HTC.

There are liquid and gas (not to be called vapor) even above the critical pressure. According to literatures of molecular dynamics, the pseudo-critical point shows the border of both and liquid and gas coexist as fluctuating spatially and temporally. Near the critical point, the gas still needs to release much energy when it changes into liquid as if vapor releases latent heat. Thus, a similar phenomenon to superheat zone condensation occurs in the supercritical heat rejection process when the pseudo-critical temperature is sandwiched between the bulk and wall temperatures.

For instance, the experimental HTC is 2.5 kW m⁻² K⁻¹ and the bulk refrigerant temperature is 31.8 °C around the pseudo-critical point of 350 kJ kg⁻¹. The temperature difference is 4 K, the tube wall temperature is 27.8°C, and the refrigerant enthalpy at 27°C is 278 kJ kg⁻¹. This means the enthalpy is radially distributed from 350 to 278 kJ kg⁻¹. This large enthalpy change is comparable to latent heat, and the HTC should be determined by the thermal properties of this averaged value. Therefore, it is not surprising that experimental HTC shows much more moderate peak than Gnielinski correlation.

Furthermore, the supercritical HTC has the maximum point above the pseudo-critical temperature (enthalpy) for the similar reason of superheat zone condensation. The tube wall

reaches a pseudo-critical point ahead of core flow in the center of tube. Goldman [22], Tanaka et al. [23], and Yamagata et al. [24] have confirmed same peak shift and that the maximum HTC appears just above the pseudo-critical temperature under cooling conditions and just below it under heating conditions.

CONCLUSIONS

Experimental results for heat rejection from CO₂ and R410A near the critical points have been provided. The predicting correlation has developed for condensing superheat zone. The results have been compared to existing correlations and newly developed correlation. The main findings are following:

- Heat rejection process is categorized as superheat, two-phase, and subcool zone by bulk mean temperature. Further, the superheat zone can be subdivided into single-phase superheat zone and condensing superheat zone based on condensation occurrence.

- Condensation starts in presence of superheated vapor when tube wall temperature reaches saturation temperature. This is demonstrated by experimental HTC, which gradually starts increasing from Gnielinski correlation [13] exactly at that point tube wall reaches saturation temperature.

- At the same reduced pressure 0.81, HTC of CO₂ is significantly higher than R410A in two-phase zone. The main reason appears to be the larger latent heat of CO₂ than R410A.

- Modified Cavallini's correlation [15], which evaluates liquid properties at the film temperature, well predicts HTC at reduced pressure up to 0.975.

- Newly developed correlation, which complements between Gnielinski's and Cavallini's correlation, has been proposed for condensing superheat zone. This correlation satisfactorily agrees with the experimental results in the range of this experiment.

- Above the critical pressure, the maximum value of experimental HTC is much lower than Gnielinski's correlation due to strong property change in radius direction. The value is closer to Petrov and Popov correlation [21] accounting for the radial property changes.

- Above the critical pressure, experimental HTC shows maximum value above the pseudo-critical temperature, because, tube wall reaches a pseudo-critical point ahead of core flow similar to condensing superheat zone.

NOMENCLATURE

C_p	isobaric heat capacity, $\text{J kg}^{-1}\text{K}^{-1}$
d_i	inner diameter of the test tube, m
f	Darcy-Weisbach friction factor in Eqs. (17) and (19)
F_a	correction factor for radial property change in Eqs. (17) and (18)
g	gravitational acceleration, m s^{-2}
G	mass flux, $\text{kg m}^{-2}\text{s}^{-1}$
h	specific enthalpy, J kg^{-1}
J_G	dimensionless vapor velocity in Eq. (15)
m	mass flow rate, kg s^{-1}
Nu	Nusselt number

P	pressure, Pa
Pr	Prandtl number
\dot{Q}	heat transfer rate, W
q	heat flux, W m ⁻²
T	temperature, °C
x_b	thermodynamic vapor quality
ΔZ_α	active cooling length of test tube, m
Δh_{LV}	latent heat, J kg ⁻¹

Greek symbols

α	heat transfer coefficient, W m ⁻² K ⁻¹
ρ	density, kg m ⁻³
λ	thermal conductivity, W m ⁻¹ K ⁻¹
μ	viscosity, Pa·s
X_{tt}	Lockhart–Martinelli parameter for turbulent phases

Subscripts

i	inlet
o	outlet
MC	mixing chamber
PC	pre-cooler

TS	test section
V	vapor
L	liquid
r	refrigerant
H ₂ O	water
w _i	interior tube wall or evaluated at interior tube wall temperature
b	evaluated at bulk temperature
f	evaluated at film temperature
sat	evaluated at saturation temperature
SH	superheat
SC	subcool
latent	latent heat
gain	heat gain from ambient air through insulations
cond	conduction heat from out of active cooling length

REFERENCES

- [1] Balekjian, G., Katz, D., Heat transfer from superheated vapors to a horizontal tube, *A.I.Ch.E. J.*, vol. 4, no. 1 pp. 43-48, 1958.
- [2] Altman, M., Staub, F. W., Norris, R. H., Local heat transfer and pressure drop for refrigerant-22 condensing in horizontal tubes, *Chem. Eng. Progress Symposium Series*. vol. 56, no. 30, pp. 151-159, 1959.

- [3] Bell, K. J., Temperature profiles in condensers, *Chem. Eng. Prog.*, vol. 68, no. 7 pp. 81-82, 1972.
- [4] Miropolsky, Z. L., Shneersva, R. I., Teernakova, L. M., Heat transfer at superheated steam condensation inside tubes, *Proc. 5th Int. Heat Trans. Conf.*, vol. 3, Tokyo, pp. 246-249, 1974.
- [5] Fujii, T., Honda, H., Nozu, S., Nakarai, S., Condensation of superheated vapor inside a horizontal tube, *Heat Transfer - Japanese Research*, vol. 4, no. 3, pp. 1-48, 1978.
- [6] Lee, C. C., Teng, Y. J., Lu, D. C., Investigation of condensation heat transfer of superheated R-22 vapor in a horizontal tube, *Proc. World Conf. Exp. Heat Trans. Fluid Mech. and Thermodynamics*, pp. 1051-1057, 1991.
- [7] Webb, R. L., Convective condensation of superheated vapor, *Trans. ASME, J. Heat transfer*, vol. 120, pp. 418-421, 1998.
- [8] Kondou, C., Hrnjak, P. S., Heat rejection from R744 flow under uniform temperature cooling in a horizontal smooth tube around the critical point, *Int. J. Refrig.*, vol. 34, no. 3, pp. 719-731, 2011.
- [9] Soliman, H.M., The mist-annular transition during condensation and its influence of the heat transfer mechanism, *Int. J. Multiphase Flow*, vol. 12, no. 2, pp. 277-288, 1986.
- [10] Lemmon, E. W., Huber, M. L., McLinden, M. O., Reference fluid thermodynamic and transport properties - REFPROP ver. 8.0, NIST, Boulder, CO, 2007.
- [11] ASME Performance Test Codes, Supplement on Instrument and Apparatus, Part1, *ASNSI / ASME PTC*, 19.1-1985, 1985.
- [12] Moffat, R. J., Description uncertainties in experimental results, *Exp. Therm. Fluid Sci.*, vol. 1,

- pp. 3-17, 1988.
- [13] Gnielinski, V., New equation of heat and mass transfer in turbulent pipe and channel flow, *Int. Chem. Eng.*, vol. 16, pp. 359-367, 1976.
- [14] Petukhov, B. S., Heat transfer and friction in turbulent pipe flow with variable physical properties, *Advances Heat Transf.*, 6, Academic Press, Orland, pp. 503-564, 1970.
- [15] Cavallini, A., Del Col, D., Doretti, L., Matkovic, M., Rossetto, L., Zilio, C., and Censi, G., Condensation in horizontal smooth tubes: a new heat transfer model for heat exchanger design, *Heat Trans. Eng.*, vol. 27, no. 8, pp. 31-38, 2006.
- [16] Sieder, E. N. and Tate, G. E., Heat transfer and pressure drop of liquids in tubes, *Ind. Eng. Chem.*, vol. 28, pp. 1429-1435, 1936.
- [17] Fujii, T., Lee, J. B., Shinzato, K., Laminar forced convection of saturated vapors in the near-critical region, *Int. J. Numer. Heat Transfer, Part A*, vol. 30, pp. 799-813, 1996.
- [18] Fujii, T., Lee, J. B., Shinzato, K., Makishi, O., Laminar free convection condensation of saturated vapors in the near-critical region, *Int. J. Numer. Heat Transfer, Part A*, vol. 31, pp. 373-385, 1997.
- [19] Nusselt, W., Die Oberflächenkondensation des wasserdampfes, *Vereines Deutscher Ingenieure*, vol. 60, no. 27, pp. 541-546, 1916. (in German)
- [20] Filonenko, G. K., Hydraulic drag in pipes, *Teploenergetika*, vol. 1, no. 4, pp. 40-44, 1954. (in Russian)
- [21] Petrov, N. E., Popov, V. N., 1985. Heat transfer and resistance of carbon dioxide being cooled in the supercritical region, *Thermal Eng.*, vol. 32, no. 3, pp. 131-134, 1985.

- [22] Goldman, K., Heat transfer to supercritical water at 5000 psi flowing at high mass flow rate through round tubes, *ASME Int. Dev. in Heat Transfer*, Part III, pp. 561-568, 1961.
- [23] Tanaka, H., Nishikawa, N., Hirata, M., Turbulent heat transfer to supercritical carbon dioxide, *Proc. 1967 Semi-Int. symp. Heat Mass Transfer*, vol.2, pp. 127-134, 1968.
- [24] Yamagata, K., Nishikawa, K., Hasegawa, S., Fujii, T., Yoshida, S., Forced convective heat transfer to supercritical water flowing in tubes, *Int. J. Heat Mass Transfer*, vol. 15, pp. 2575-2593, 1972.

Table 1 Measurement uncertainties

Nomenclature	Instrument	Uncertainty
T_{rb}, T_{H_2O}	Sheathed T type Thermocouple	± 0.05 K
T_{wi}	Twisted T type Thermocouple	± 0.10 K
P_{MC}	Diaphragm absolute pressure transducer	± 0.05 MPa
ΔP	Diaphragm differential pressure transducer	± 0.26 kPa
$\dot{m}_{H_2O, TS}, \dot{m}_r$	Coriolis mass flow meter	± 0.1 g s ⁻¹
$\dot{m}_{H_2O, PC}$	Coriolis mass flow meter	± 0.5 g s ⁻¹

LIST OF FIGURES CAPTIONS

Figure 1 Heat flow and temperature distribution in the condensing superheat zone

Figure 2 Experimental apparatus

Figure 3 Specifications of the test section and test tube

- (a) Test section
- (b) Dimensions of the test tube
- (C) Data reduction procedure

Figure 4 Comparison between experimental results and predictions for HTC

(Dashed lines: existing correlations by Cavallini et al. [15] and Gnielinski [13], Solid lines: proposed correlation Eqs. (15) to (19))

- (a) R410A, 2.7 MPa, $P/P_{\text{crit}} = 0.55$, $200 \text{ kg m}^{-2}\text{s}^{-1}$, 10 kW m^{-2}
- (b) R410A, 4.0 MPa, $P/P_{\text{crit}} = 0.81$, $100 \text{ kg m}^{-2}\text{s}^{-1}$, 10 kW m^{-2}
- (c) CO₂, 6.0 MPa, $P/P_{\text{crit}} = 0.81$, $100 \text{ kg m}^{-2}\text{s}^{-1}$, 10 kW m^{-2}

Figure 5 Change in HTC towards the critical points

- (a) CO₂, $100 \text{ kg m}^{-2}\text{s}^{-1}$, 10 kW m^{-2}
- (b) R410A, $100 \text{ kg m}^{-2}\text{s}^{-1}$, 10 kW m^{-2}

Figure 6 Example of specific heat distribution in liquid film

Figure 7 Overview of calculation procedure

Figure 8 Experimental HTC of various heat fluxes and proposed correlations

- (a) CO₂, 6.0 MPa, $100 \text{ kg m}^{-2}\text{s}^{-1}$

(b) R410A, 2.7 MPa, $200 \text{ kg m}^{-2}\text{s}^{-1}$

Figure 9 Comparison on HTC between CO₂ and R410A at the same reduced pressure

(Symbol: experiment, dashed line: existing correlations by Cavallini et al. [15] and Gnielinski [13], solid line: proposed correlation Eqs. (15) to (19))

Figure 10 Summary of experimental HTC and correlation

(Symbol: experiment, solid lines: proposed correlations Eqs. (15) to (19) at subcritical pressures and correlations by Gnielinski [13] and Petrov and Popov [21] at the supercritical pressure.)

(a) CO₂, $100 \text{ kg m}^{-2}\text{s}^{-1}$, 10 kW m^{-2}

(b) R410A, $200 \text{ kg m}^{-2}\text{s}^{-1}$, 10 kW m^{-2}

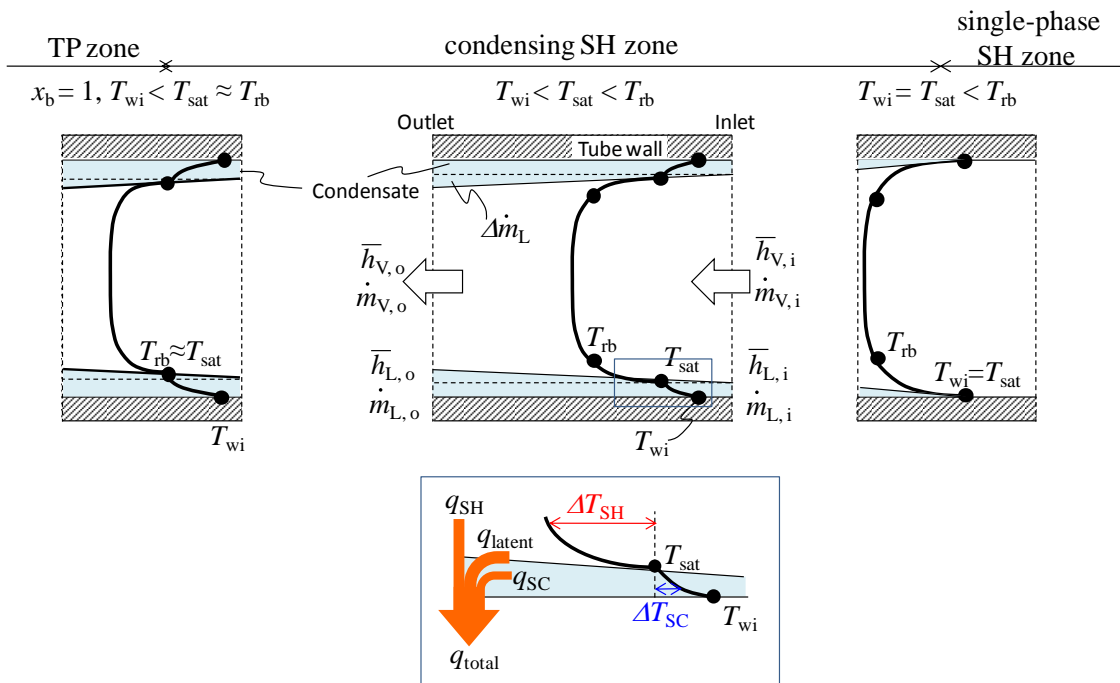


Figure 1 Heat flow and temperature distribution in the condensing superheat zone

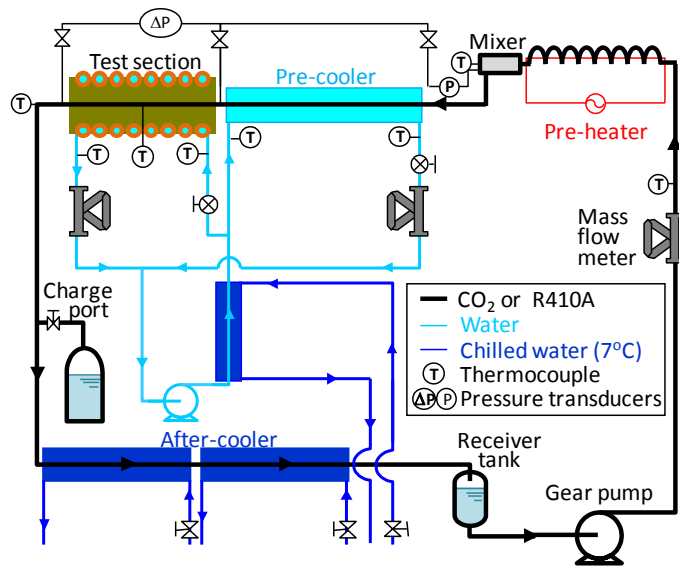
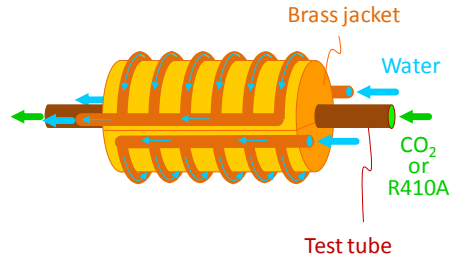
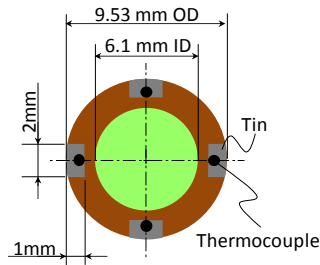


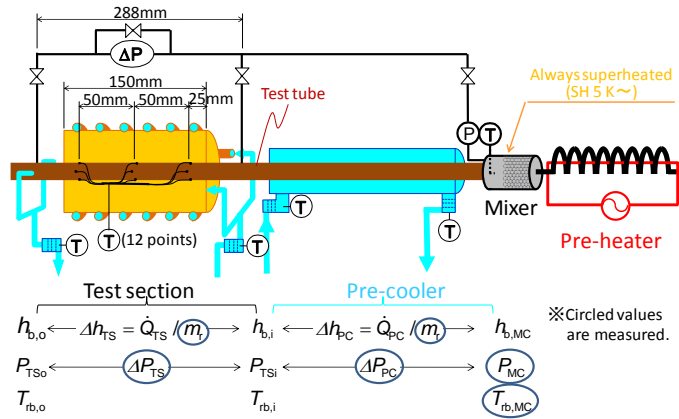
Figure 2 Experimental apparatus



(a) Test section



(b) Dimensions of the test tube



(C) Data reduction procedure

Figure 3 Specifications of the test section and test tube

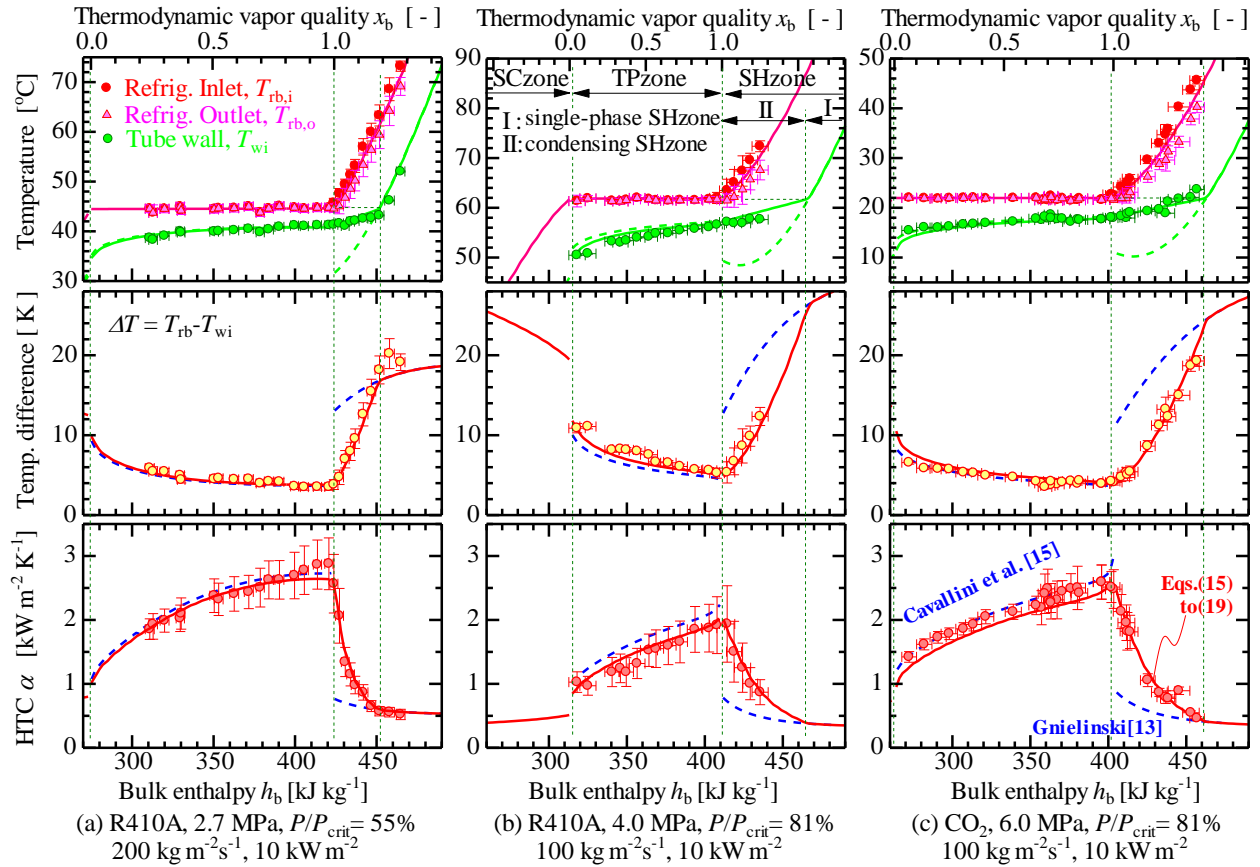


Figure 4 Comparison between experimental results and predictions for HTC
(Dashed lines: existing correlations by Cavallini et al. [15] and Gnielinski [13], Solid lines: proposed correlation Eqs. (15) to (19))

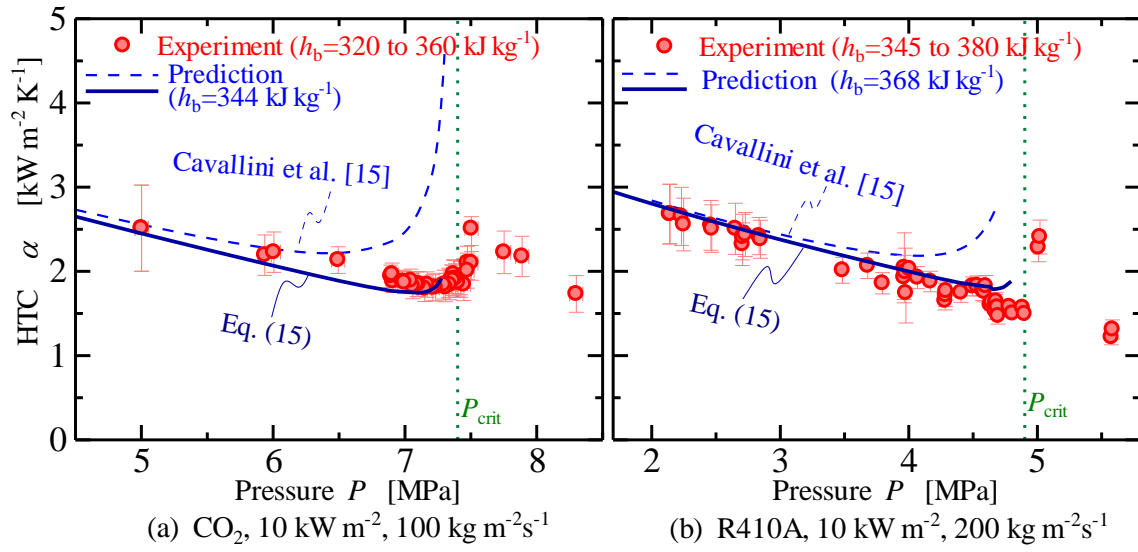


Figure 5 Change in HTC towards the critical points

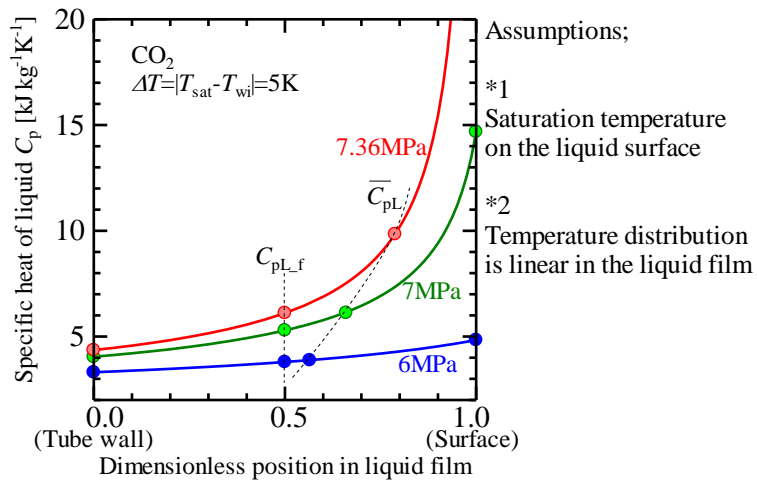


Figure 6 Example of specific heat distribution in liquid film

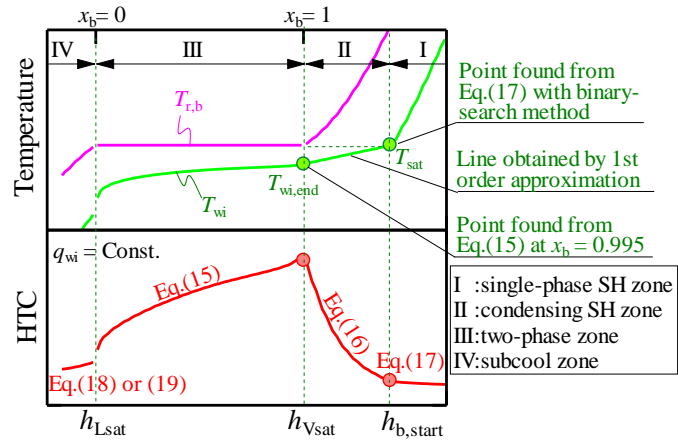
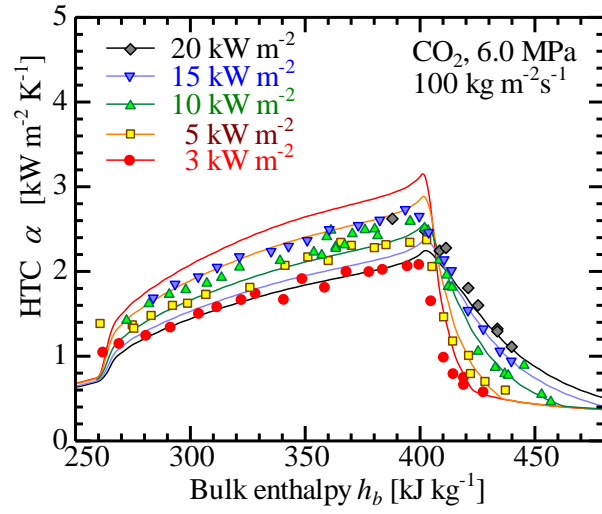
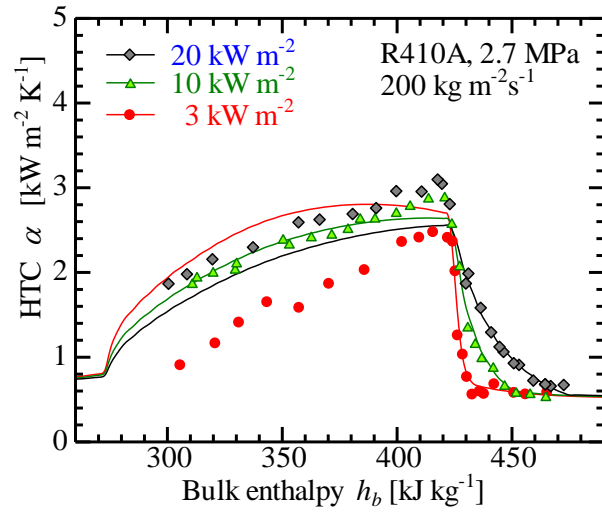


Figure 7 Overview of calculation procedure



(a) CO₂ at 100 kg m⁻²s⁻¹



(b) R410A at 200 kg m⁻²s⁻¹

Figure 8 Experimental HTC of various heat fluxes and proposed correlations

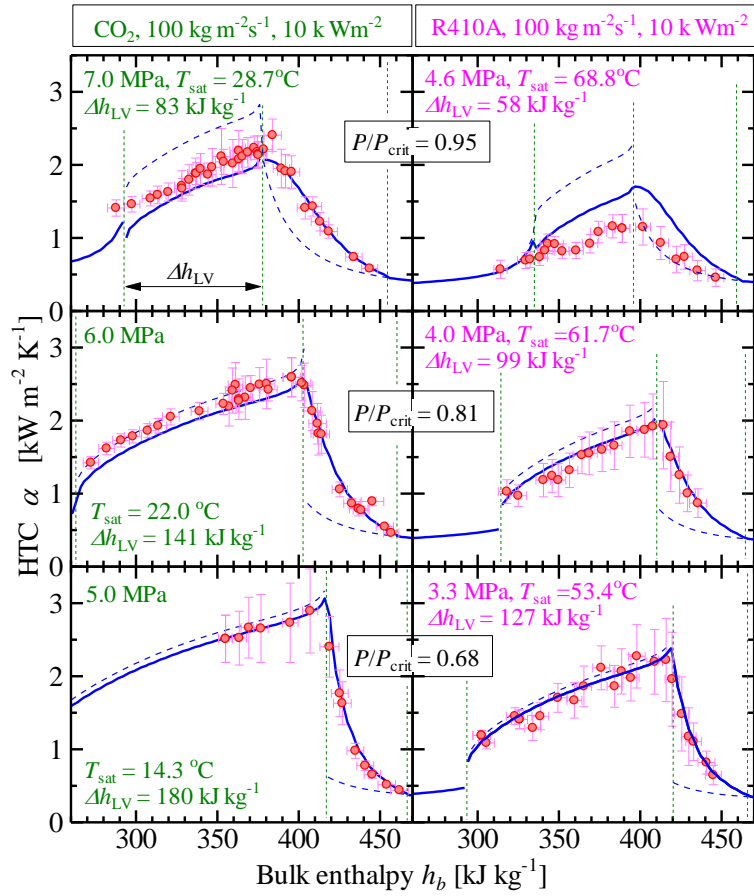
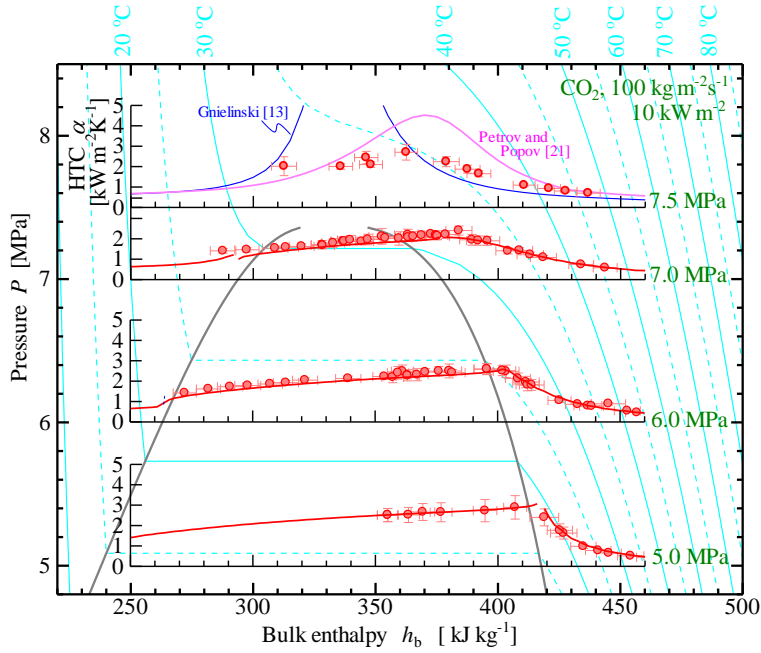
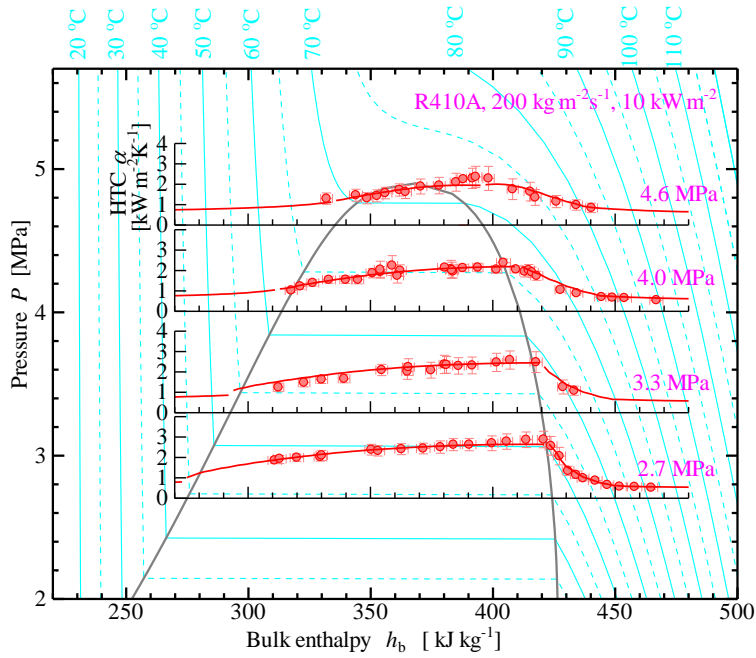


Figure 9 Comparison on HTC between CO₂ and R410A at the same reduced pressure (Symbol: experiment, dashed line: existing correlations by Cavallini et al. [15] and Gnielinski [13], solid line: proposed correlation Eqs. (15) to (19))

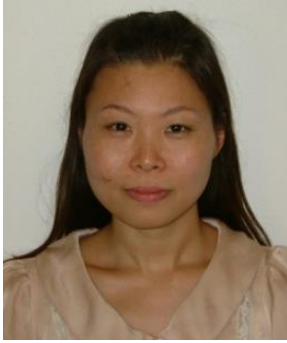


(a) CO_2 , $100 \text{ kg m}^{-2}\text{s}^{-1}$, 10 kW m^{-2}



(b) R410A , $200 \text{ kg m}^{-2}\text{s}^{-1}$, 10 kW m^{-2}

Figure 10 Summary of experimental HTC and proposed correlation
(Symbol: experiment, solid lines: proposed correlations Eqs. (15) to (19) at subcritical pressures and correlations by Gnielinski [13] and Petrov and Popov [21] at the supercritical pressure.)



Chieko Kondou is a visiting scholar at Air Conditioning and Refrigeration Center (ACRC) in University of Illinois, Urbana-Champaign, USA. She worked on development of higher efficient air conditioners and commercial refrigeration systems in Hitachi Appliances Inc. for seven years, and received her PhD from Kyushu University, Japan.



Pega Hrnjak is Co-Director of the Air Conditioning and Refrigeration Center (ACRC), the University of Illinois at Urbana Champaign, NSF founded university – industry cooperative research center, home for over 100 researchers focused on system aspects, components, interaction, controls of modern energy conversion systems, fully funded by contributions of 30 world leading companies. Prof. Hrnjak's 25 students strong research group is an integral part of the ACRC. Pega is also a founder and president of a vibrant R&D company CTS which bridges ACRC activities (precompetitive research in function of education) and industry with its typically confidential program conducted by 50 full time engineers and scientists in a 6000 m² own laboratory facility. Prof. Hrnjak advised over 70 graduate students so far and authored or coauthored with them over 250 articles, wrote chapters in several books, and made numerous lectures worldwide. Pega is active member of ASME, ASHRAE (Fellow), IIR, SAE, IIAR (past Board of Directors member), was and is editor or member of the boards of several professional journals. Before joining faculty of the University of Illinois in 1993 Pega started his

academic journey at the University of Belgrade, with appointments at few other universities along his career.